Hydrogeology Journal (2019) 27:2581–2593
https://doi.org/10.1007/s10040-019-02011-1

REPORT

Sequential indicator simulation for a three-dimensional distribution of hydrofacies in a volcano-sedimentary aquifer in Mexico City

Priscila Medina-Ortega[1] · Eric Morales-Casique[2] · Antonio Hernández-Espriú[3]

Received: 21 August 2018 / Accepted: 22 June 2019 / Published online: 6 July 2019

Abstract

The Mexico City aquifer is a complex mix of alluvial deposits and volcanic rocks overlapped by an aquitard composed of lacustrine deposits. To characterize this heterogeneous hydrogeologic system, a three-dimensional model of the distribution of hydrofacies is constructed using borehole lithological records. The analysis is based on 111 borehole logs with an average depth of 300 m, in an area of 234 km^2, providing a nominal scale of resolution of 2.1 km in the plane and 2-m resolution in the vertical direction. These records were discretized to generate a georeferenced dataset of 13,518 points associated with a lithological category; nine lithological categories were observed. These categories were subsequently grouped into four hydrofacies: A and B, grouping low-permeability lithological categories (lacustrine and volcano-sedimentary materials, respectively); and C and D, grouping high-permeability lithological categories (volcanic rocks and alluvial deposits, respectively). The database was analyzed in terms of proportion of hydrofacies at depth, distribution of layer thickness, and behavior of experimental horizontal and vertical variograms. The experimental variograms of each hydrofacies were fitted to exponential models via minimization of cross-validation errors. Three-dimensional models of probability of occurrence of each hydrofacies and the combined distribution of hydrofacies were then constructed via ensemble averaging of 1,000 realizations obtained by sequential indicator simulation. The potential use of this model for water management, modeling land subsidence, and groundwater pollution is discussed.

Keywords Indicator geostatistics · Hydrofacies · Aquifer heterogeneity · Lithological logs · Mexico

Introduction

Mexico City is one of the most populated cities in the world and the urban concentration causes diverse problems such as shortage of water supply, land subsidence and groundwater pollution. The Mexico City aquifer is a complex mix of alluvial deposits and volcanic rocks, and supplies 66% of the ~62 m^3/s of water required in the Basin of Mexico (Hernández-Espriú et al. 2014; Escolero et al. 2016). This aquifer is overlapped by a lacustrine aquitard composed mainly of highly compressible clayey materials described as allophanes (Carreón-Freyre et al. 2010; Jaime-P and Méndez-Sánchez 2010). Groundwater pumping has caused severe land subsidence in Mexico City at rates that have exceeded 0.4 m/year and more than 13.5 m of subsidence has accrued since the 1930s (Ortega-Guerrero et al. 1999; Auvinet 2009); maximum rates of nearly 0.35 m/year have been recently measured (Cabral-Cano et al. 2008). In order to face these challenges and to propose alternative water management policies, sound hydrogeological modeling of this system is needed. These modeling efforts need to consider, among other aspects, the natural heterogeneity of the geological formations. Lateral and vertical heterogeneity in this hydrogeological system has important effects when modeling land subsidence due to groundwater pumping (Hernández-Espriú et al. 2014; Zapata-Norberto et al. 2018), to model ground fracturing due to differential settlement (Carreón-Freyre et al. 2010, 2011; Hernández-Espriú et al. 2014), in contamination and vulnerability studies (Hernández-Espriú et al. 2014; Domínguez-Mariani et al. 2015) and in predicting and modeling the seismic response of a given site to an earthquake (Avilés and Pérez-Rocha 2010; Arroyo et al. 2013;

✉ Eric Morales-Casique
ericmc@geologia.unam.mx

[1] Posgrado en Ciencias de la Tierra, Universidad Nacional Autónoma de México, C.P. 04510 Ciudad de México, Mexico

[2] Instituto de Geología, Universidad Nacional Autónoma de México, C.P. 04510 Ciudad de México, Mexico

[3] Hydrogeology Group, Facultad de Ingeniería, Universidad Nacional Autónoma de México, C.P. 04510 Ciudad de México, Mexico

Ovando-Shelley et al. 2013). Despite this need, a tridimensional model of this aquitard-aquifer system, defining lateral and vertical heterogeneity up to the depth of the production wells, that is, up to several hundred meters depth, is not existent for Mexico City.

Adequate representation of spatial heterogeneity is challenging due to the typically high variability in aquifer properties such as hydraulic conductivity *K*. In granular aquifers, the spatial distribution of *K* is typically related to the distribution of lithofacies, i.e., a mappable subdivision based on lithology of a main stratigraphic unit. In the framework of spatially correlated random variables, the boundary between two lithofacies likely defines the boundary between two regions, each one with its own probability density function of *K* (Ritzi 2000). The concept of hydrofacies has been introduced to improve the representation of spatial variability and to enable the incorporation of soft geological data. A hydrofacies groups lithofacies which have similar hydraulic properties, mainly *K* (Johnson and Dreis 1989; Poeter and Gaylord 1990; Johnson 1995). The concept of hydrofacies is particularly valuable because lithologic data are often more abundant and readily available than *K* data.

The distribution of hydrofacies is frequently analyzed using a geostatistical framework so that the uncertainty related to incomplete knowledge of the subsurface (due to sparse measurements and measurement errors) can be incorporated into the modeling framework. The indicator geostatistics approach is an alternative that provides a quantitative way to characterize, delineate and simulate the spatial distribution of hydrofacies. The indicator approach was introduced by Journel (1983) and further extended by others to assess, infer, or simulate the spatial distribution of hydrofacies (Ritzi et al. 1994; Carle and Fogg 1996, 1997; Fogg et al. 1998; Ritzi 2000; Ritzi et al. 2000; dell'Arciprete et al. 2012). Within this strategy, an indicator function can take (at any given point in space) the value zero or one, depending on whether the point is inside, or outside a given facies.

Hard data (such as *K* measurements) to characterize aquifer heterogeneity are difficult and expensive to collect, while soft data (such as borehole lithological records) are sometimes more abundant, but they are not easily related to quantitative parameters such as hydraulic conductivity. Despite this limitation, borehole data is helpful in delineating aquifer heterogeneity. Indicator methods are attractive as a means of addressing the categorical nature of geologic data and for incorporating the geometric context of geologic facies. Johnson (1995) employed indicator variograms to characterize the distribution of two hydrofacies in an alluvial fan setting. Ritzi et al. (2000) applied indicator characterization to two buried-valley aquifers, composed of glaciofluvial sediments. The lithological categories were grouped in two hydrofacies: a predominantly sand and gravel lithofacies (facies s) interbedded with a mud and diamicton lithofacies (facies m). Moysey et al. (2003) employed sequential indicator simulation to generate facies realizations conditioned to radar facies probabilities. Considerable research has been carried out to investigate how borehole data can contribute to improve the depiction of spatial heterogeneity in groundwater systems (Ezzedine et al. 1999; He et al. 2014; Jørgensen et al. 2015).

The aim of this work is to characterize the spatial heterogeneity of the southern portion of the hydrogeologic system in Mexico City. The approach employed is based on sequential indicator simulation of hydrofacies defined from lithological records of groundwater wells. Sequential indicator simulation was chosen because it is a very efficient algorithm and allows to easily mix hard and soft data. The lithological categories in the borehole records were grouped and categorized into four hydrofacies (two pairs of high and low hydraulic conductivity hydrofacies, one pair for volcanic rocks and one for sedimentary deposits) and analyzed using indicator functions to discover spatial relations among them. Thus, the approach employed illustrates the application of sequential indicator simulation to four variables, a step forward from the typical application to two variables.

Hydrogeological setting

The Basin of Mexico, located in the Trans-Mexican Volcanic Belt, is a structure with more than 2,000 m of sedimentary fillings and mostly Miocene to Quaternary volcanic rocks (Vázquez-Sánchez and Jaimes-Palomera 1989; Arce et al. 2013, 2015, 2019). The study area is 234 km^2 and is located at the southern part of the basin (Fig. 1). The volcanic rocks in the study area belong to the Chichinautzin volcanic field, of Pleistocene-Holocene age, and the Sierra de Las Cruces volcanic sequence, of Pliocene-Pleistocene age (Fig. 1; Arce et al. 2015, 2019). The Chichinautzin volcanic field forms part of the southern limit of the Basin of Mexico and is comprised of more than 120 monogenetic volcanoes (Arce et al. 2015). In the study area (Fig. 1) this field includes the units Sierra Santa Catarina, Cerro de la Estrella and Peñón del Marqués (Arce et al. 2015, 2019). The Cerro de la Estrella volcano is located almost at the center of the study area (Fig. 1), and is a "shield volcano" due to the very soft slopes and edges of its radial lava fronts and is crowned by a cone of scoria (Arce et al. 2015). The Sierra Santa Catarina is formed by seven monogenetic volcanic structures, aligned in the general direction E–W; most of these structures are ash and slag cones with associated lava flows, one is a lava dome and the western structure is a maar (Arce et al. 2015). Peñón del Marqués is also a monogenetic volcano (Arce et al. 2015). These volcanic rocks are sometimes covered or interbedded with alluvial and fluviatile materials (Vázquez-Sánchez and Jaimes-Palomera 1989; García-Palomo et al. 2008; Arce et al. 2015).

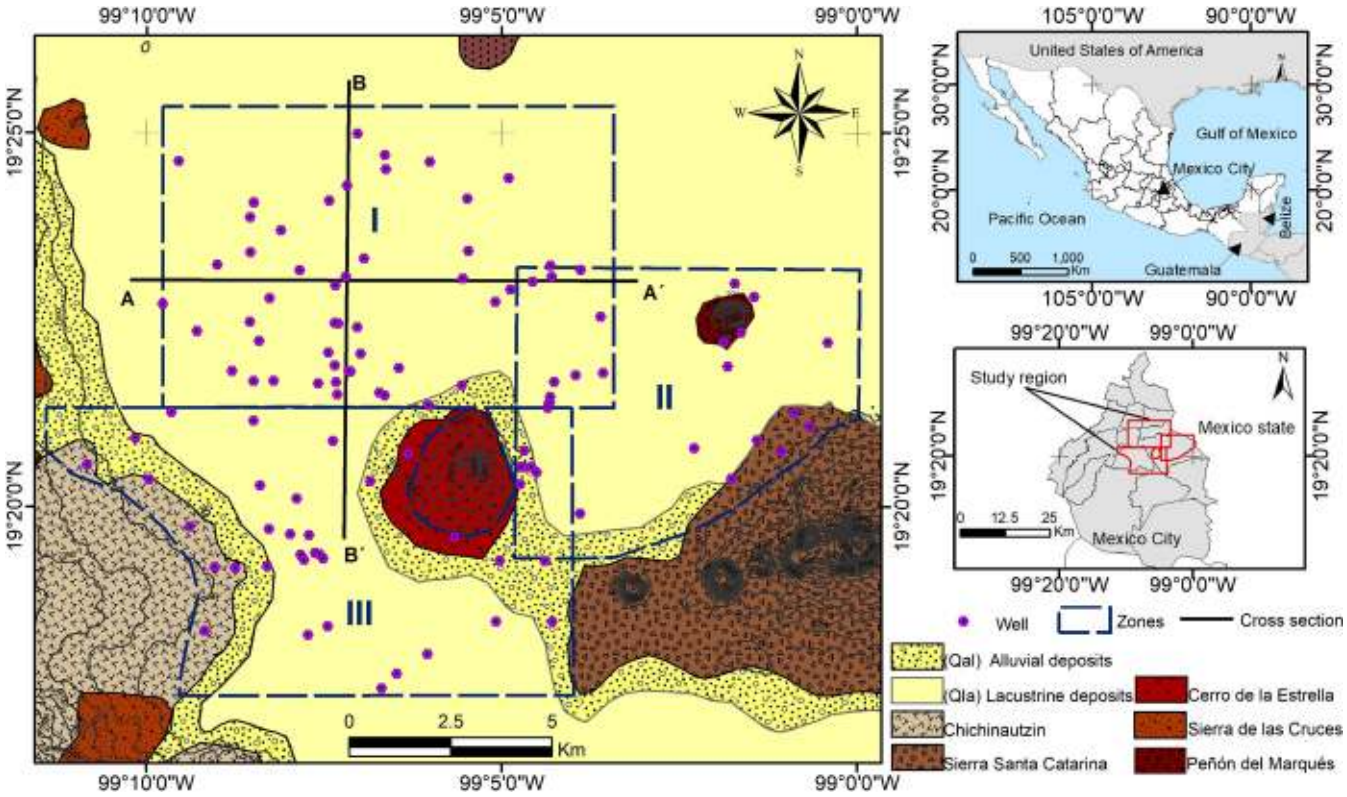

Fig. 1 Geographical and geological setting of the study area in Mexico (adapted from Vázquez-Sánchez and Jaimes-Palomera 1989 and Arce et al. 2015, 2019). Symbols correspond to groundwater wells with available lithological records

The surface geology (Fig. 1) also includes lacustrine (Qla) and alluvial deposits (Qal), which are interbedded at their contact, and are also frequently interbedded with the volcanic and volcaniclastic deposits (Vázquez-Sánchez and Jaimes-Palomera 1989; Arce et al. 2015, 2019). Lacustrine sediments in Mexico City consist of a 60–100-m-thick section of clay (Marsal and Mazari 1959), reaching up to 300 m in thickness in Chalco, outside of Mexico City (Lozano-García et al. 2017). Interbedded with these sediments are layers of volcaniclastic material of a few centimeters in thickness (Ortega-Guerrero et al. 2017). In some areas of the city, these volcaniclastic layers reach a few meters in thickness, are composed of sands, gravely sands, silts, sandy silts and thin lenses of silty clays, and are known in the geotechnical literature as *capas duras* or hard layers (Marsal and Mazari 1959; Ovando-Shelley et al. 2013; Mooser 2018).

In a simplified hydrogeological conceptual model, the alluvial/clastic/volcanic materials constitute the aquifer supplying groundwater to Mexico City, overlapped and semiconfined by the clayey aquitard constituted by the lacustrine unit (Hernández-Espriú et al. 2014; Morales-Casique et al. 2015). Average depth of groundwater wells is 200 m, with a few of them reaching up to 1,000 m (Escolero et al. 2016).

Methods

Lithological records

Lithological records from groundwater wells were obtained from the databases of the National Water Agency (CONAGUA), the Federal Power Agency (CFE), the Mexican Oil Company (PEMEX) and the Water Supply Agency of Mexico City (SACMEX) and from Valencia-Cruz (2002). A total of 111 lithological records were obtained having an average depth of ~300 m and containing 11 lithological categories (Figs. 1 and 2), or about one well per 2.1 km^2. This data density leads to a nominal resolution scale of 1.45 km; however, since data density is not uniform (Fig. 1), some areas have a finer resolution, while others have a coarser resolution. The lithological records were discretized in intervals of 2 m and the corresponding lithological category was assigned to the center of the interval. Based on data availability and considering topographic elevation of each well, a common depth interval for all lithological records of 300 m was selected for the analysis.

Definition of hydrofacies

To simplify the problem, the lithological categories were grouped in four hydrofacies denoted A, B, C and D.

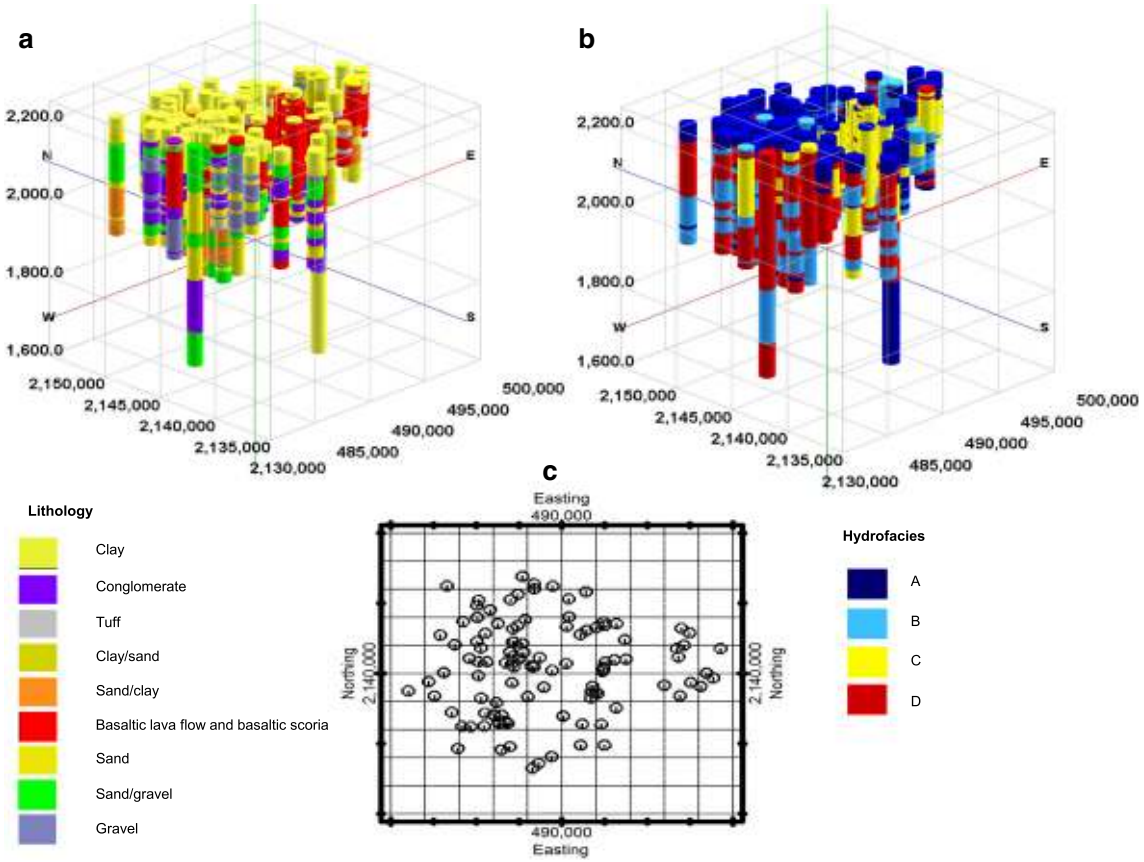

Fig. 2 **a** Lithology records of the groundwater wells and **b** distribution of hydrofacies. **c** Locations of wells with lithological records are shown

Hydrofacies A and B group low hydraulic conductivity sediments and volcanic materials. Hydrofacies C and D group high hydraulic conductivity volcanic rocks and sediments, respectively. The vertical resolution in the definition of hydrofacies was kept equal to 2 m. An indicator function was then assigned to the hydrofacies data

$$I_i(x,y,z) = \begin{cases} 1 & (x,y,z) \in \text{hydrofacies } i \\ 0 & \text{otherwise} \end{cases} \quad (1)$$

Discretization of the 111 borehole logs resulted in 13,518 data. Global variability of hydrofacies was analyzed by computing proportions at different depths. The proportion of hydrofacies i at elevation z_l is computed as

$$P_{\mathrm{pi}}(z_l) = \frac{1}{N} \sum_{j=1}^{N_w} \sum_{k=1}^{N_{k,j}} I_i\left(x_j, y_j, z_l - \Delta z \le z \le z_l + \Delta z\right) \quad (2)$$

where I_i is the indicator function of hydrofacies i, N_w is the number of wells, $N_{k,j}$ is the number of data of the j-th well between the limits $z_l \pm \Delta z$, and N is the total number of data between the same limits $z_l \pm \Delta z$, for all wells. In case $N_{k,j}$ is constant for all wells, $N = N_w\, N_{k,j}$; however, since each well has a different topographic elevation, in general $N_{k,j}$ is different for each well.

Variogram modeling

The Cerro de la Estrella volcano is located roughly at the center of the area (Fig. 1); there are no wells on this structure, and thus no information about its structure at depth. To avoid extrapolating across the volcano, and for computational convenience, the area was divided into three zones: I, II and III (Fig. 1). Each zone was modeled separately. Experimental variograms for each hydrofacies were computed at each zone for two directions, horizontal and vertical. An exponential model was fitted to the experimental variogram of each hydrofacies. The variograms parameters were obtained by minimizing the cross-validation errors using PEST 12.2 (Doherty 2010). Five-fold cross-validation errors were computed using GSLIB (Deutsch and Journel 1998) and the three estimated parameters for each hydrofacies were sill and integral scale in the vertical and horizontal directions.

Sequential indicator simulation

A total of 1,000 realizations of each hydrofacies were generated by sequential indicator simulation using GSLIB (Deutsch and Journel 1998). The exponential correlation structure and the corresponding parameters were those obtained from the

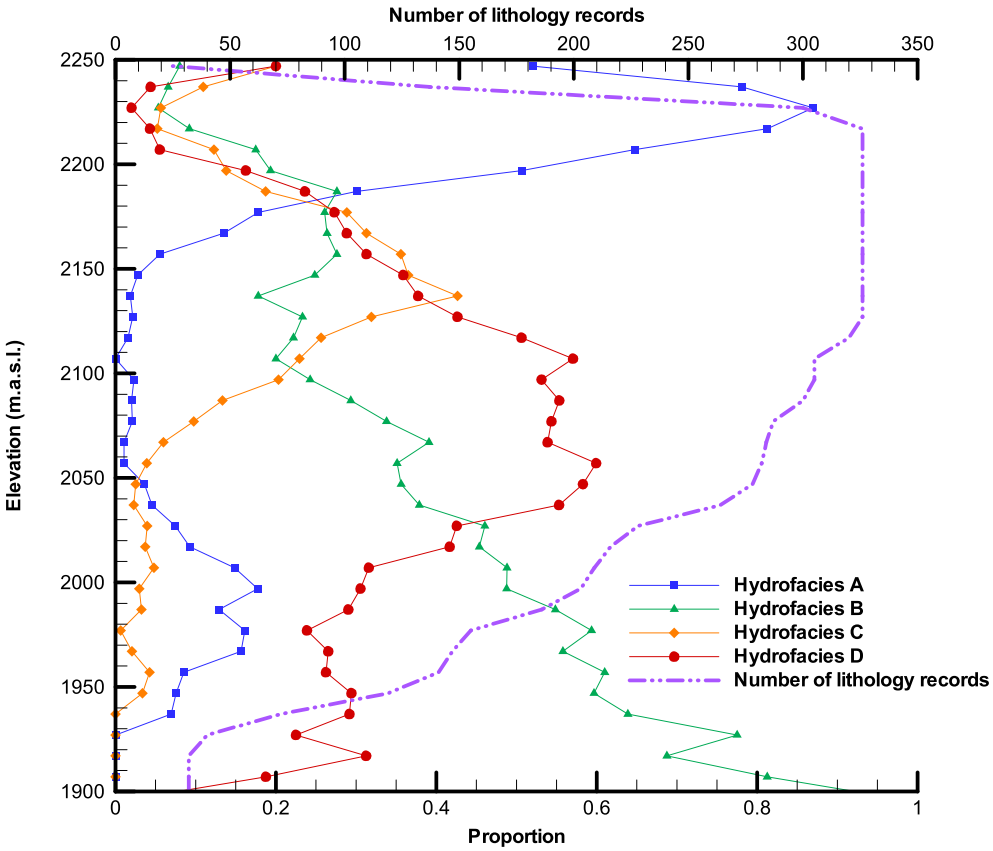

Fig. 3 Proportion of hydrofacies with topographic elevation: A – low-*K* lacustrine clay, B – low-*K* volcanic and volcano sedimentary materials, C – high-*K* volcanic rocks and D – high-*K* alluvial sediments

variogram modeling step. The realizations were averaged to compute probability of occurrence for each hydrofacies. Point convergence of these averages was verified at random locations. The average results were then combined, assigning the hydrofacies with the largest probability of occurrence at each point. Boundary locations between hydrofacies, where two or more of them had similar probabilities of occurrence, were solved last by combining a nearest neighbor algorithm to identify the closest hydrofacies and a decision rule to preserve the proportion of hydrofacies at the elevation z_i. That is, the location in question was assigned to hydrofacies i if $[P_{pi}(z_l)]_{real} > [P_{pi}(z_l)]_{simulated}$, trying to preserve the global proportion of hydrofacies. Based on this procedure, a tridimensional model of the distribution of hydrofacies was generated. The spatial discretization of the hydrofacies models is (x, y, z): zone I (109, 69 and 4.5 m), zone II (229, 136 and 7 m) and zone III (161, 137 and 7 m), where x is the E–W direction, y is N–S direction and z is elevation.

Table 1 Variogram parameters for each hydrofacies at the three zones

Hydrofacies	Nugget	Sill	Integral scale	
			Horizontal (m)	Vertical (m)
Zone I				
A	0.15	0.08	1,212.8	40
B	0.13	0.11	1,341.3	35.7
C	0.09	0.05	700.0	23.5
D	0.13	0.09	439.2	24.6
Zone II				
A	0.02	0.1	800.8	45.0
B	0.01	0.14	691.0	32.4
C	0	0.15	385.9	29.5
D	0	0.25	107.0	14.1
Zone III				
A	0.04	0.18	824.4	22.0
B	0.07	0.1	426.3	25.0
C	0.1	0.15	88.0	47.0
D	0.03	0.11	115.0	21.6

Results

Lithological categories and hydrofacies

The 111 lithological records contained 11 types of sediments/rocks—namely clay, clay-sand, sand, sand-clay, sand-gravel, basaltic lava flow, scoria, conglomerate, gravel and tuff (Fig. 2). Total depth of the lithological logs varies from 100 m to over 1,000 m, with most wells having depths between 200–300 m. Thickness of the lacustrine clay varies from 10 to

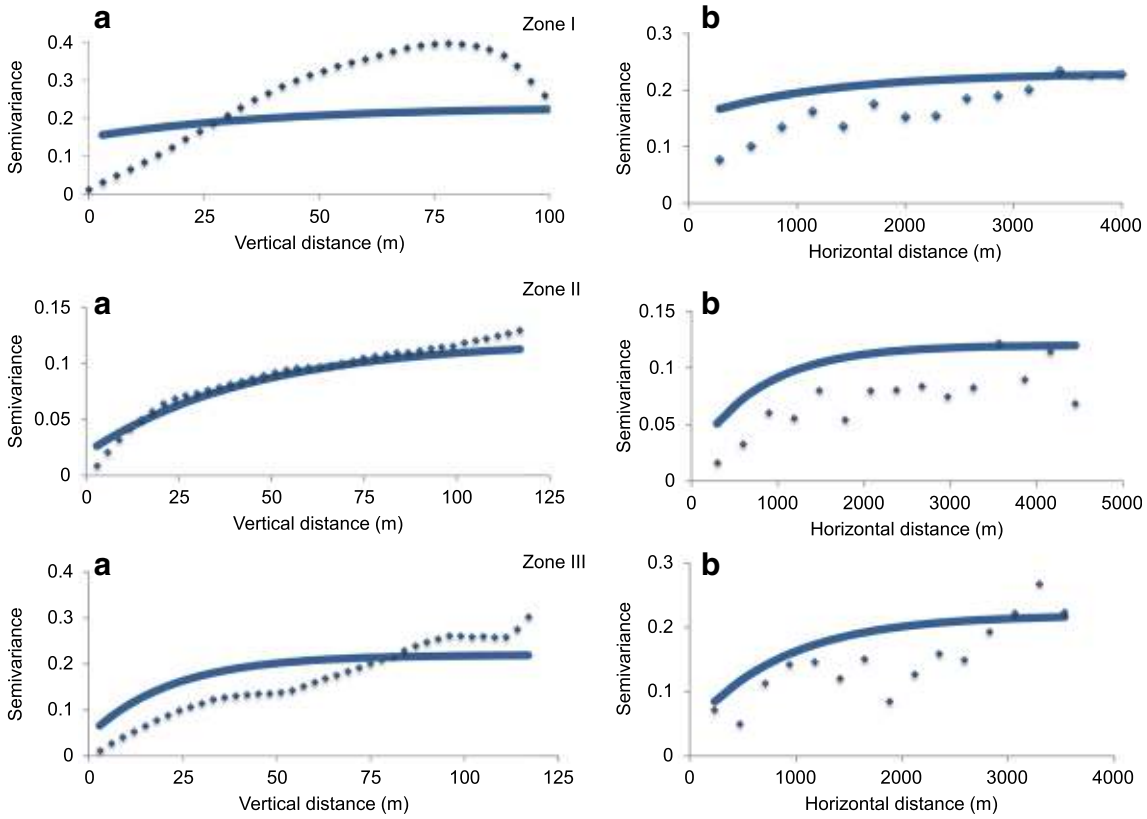

Fig. 4 **a** Vertical and **b** horizontal variograms for hydrofacies A in zones I, II and III. Symbols represent the experimental variogram and lines are the fitted models

65 m. Figure 2 also depicts the spatial distribution of the four hydrofacies in groundwater wells. Each hydrofacies was defined by grouping one or more of the lithologic categories depending on its estimated hydraulic conductivity and its primary or secondary porosity.

Hydrofacies A is characterized by the main presence of low-*K* lacustrine clay that constitutes the upper aquitard of the hydrogeologic system with thicknesses of 6–70 m in the study area. Hydrofacies B groups clay-sand, conglomerate, sand-clay and tuff. Tuffs in this area are typically altered into clay (Dirección General de Construcción y Operación Hidráulica, Estudio y cuantificación de caudales de los manantiales del Poniente, Mexico City, unpublished report, 1992). These materials are considered low-*K* alluvial and volcanic deposits. Hydrofacies C groups lava flows and scoria and is considered of high-*K* due to secondary porosity. Finally, hydrofacies D groups alluvial deposits of high-*K*: sand, gravel and sand-gravel. Hydrofacies D is interbedded with hydrofacies B and to less extension with hydrofacies C; these three hydrofacies constitute the main aquifer under exploitation in Mexico City.

Figure 3 depicts the proportion of each hydrofacies with depth. Proportion of hydrofacies A varies from 60 to 80% in the first 60 m, decreasing to only ~5% at an elevation of 2,150 masl. Hydrofacies B varies almost linearly from 5 to 55% in the range of 2,250 masl to 1,950 masl and is relatively more abundant (proportions from 40 to 55%) from 2,050 masl downwards. Hydrofacies C is mainly found from 2,200 to 2,080 masl with proportions from 15 to 50% (maximum at 2,130 masl). Hydrofacies D predominates from 2,150 to 2,000 masl with proportions from 30% to a maximum of 60% at an elevation of 2,050 masl (Fig. 3).

Overall, the main aquifer (roughly from 2,170 to 1,920 masl; ~230 m thick) is composed mainly of high-*K* hydrofacies D (30−50%), while hydrofacies C is more abundant in the first 100 m (about 25% in average, but peaking at 50% around 2140 masl), while low-K hydrofacies B is more abundant (30–50%) in the bottom 100 m.

Variograms

Variogram parameters for each hydrofacies at the three zones are presented in Table 1. Hydrofacies A (lacustrine clayed sediments) and B (low-*K* alluvial and volcanic deposits) present the longest horizontal integral scale. Hydrofacies C and D (high-*K* volcanic rocks and alluvial deposits, respectively) resulted in shorter horizontal integral scales than the low-*K* hydrofacies (Table 1). Vertical integral scale of low-*K* hydrofacies (A and B) are longer than the corresponding to the high-*K* hydrofacies, except

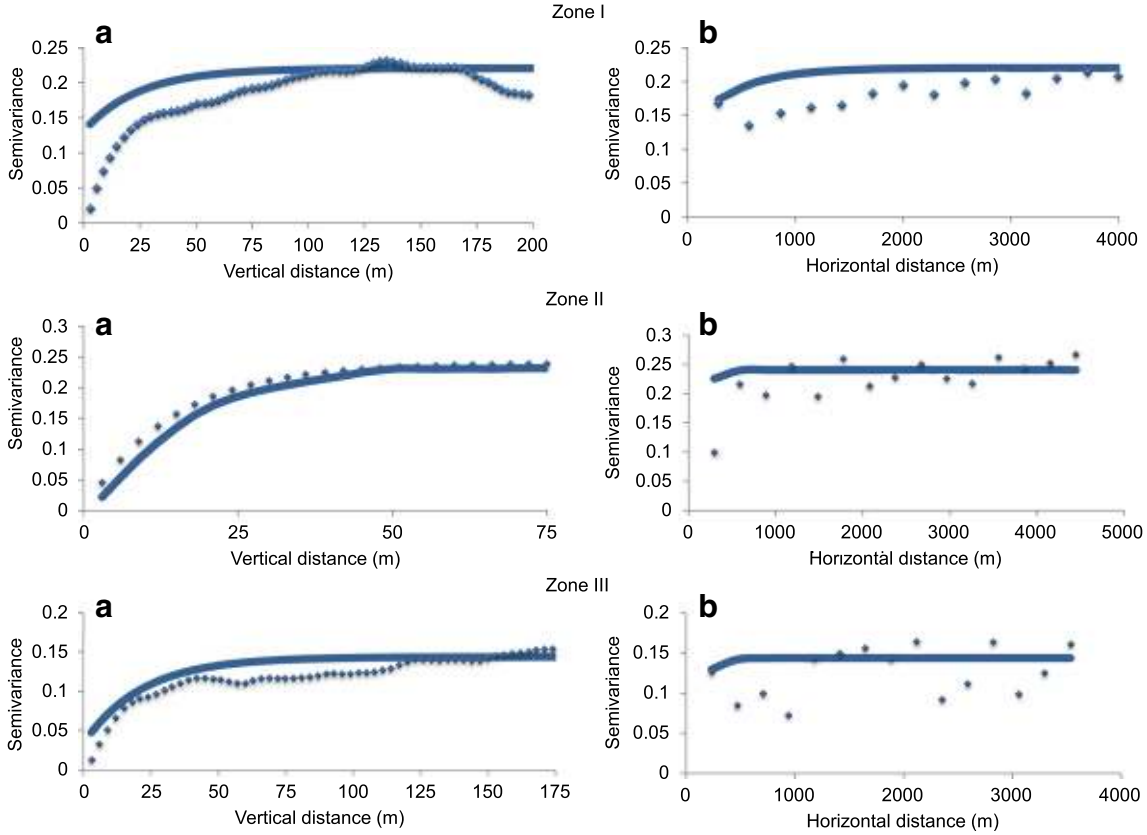

Fig. 5 **a** Vertical and **b** horizontal variograms for hydrofacies D in zones I, II and III. Symbols represent the experimental variogram and lines are the fitted models

for zone III where occurs the opposite. Fitted variograms for hydrofacies A and D in the three zones are depicted in Figs. 4 and 5, respectively. Zonal anisotropy between the vertical and horizontal directions occurs for hydrofacies A in zones I and II (Fig. 4), and for hydrofacies B and C in zone I (not shown). Variograms for zone III did not present zonal anisotropy (Fig. 5).

Vertical integral scale in Table 1 can be roughly related to the average thickness of each hydrofacies. For hydrofacies A, this integral scale can be related to the average thickness of the semiconfining layer in the study zones, from 22 m in zone III, to 45 m in zone II. Average thickness of hydrofacies D goes from 14 m in zone II to about 25 m in zone I, which is consistent with the conceptual model where hydrofacies D is interbedded with hydrofacies B and C.

Three-dimensional model of hydrofacies

Figure 6 depicts the resulting three-dimensional (3D) model of distribution of hydrofacies for the three zones, as obtained by averaging 1,000 realizations using the sequential indicator simulation. As expected, hydrofacies A, corresponding to lacustrine sediments, is almost continuous in the upper portion of each zone. It is evident that the 3D model, and the available lithological records from groundwater wells, do not have the vertical resolution to define the tephra layers interbedded with the clayey lacustrine sediments. Hydrofacies A represents the aquitard that semiconfines the main aquifer, currently under intensive development. Overall, hydrofacies A reaches a thickness up to ~100 m; in addition, discontinuous lenses of this hydrofacies appear deeper, particularly in zones I and III, according to Fig. 6. It is inferred that these deeper lenses are not related to the lacustrine aquitard, and are interbedded with volcanic rocks, i.e., volcaniclastic deposits, previously reported by other authors, as a common feature of the basin's geology (Carrera-Hernández and Gaskin 2008; García-Palomo et al. 2008).

On the other hand, the main aquifer is comprised of hydrofacies C and D related to fractured-based volcanic rocks and alluvial/fan deposits, respectively, and of hydrofacies B, composed of less permeable clastic/pyroclastic deposits. Hydrofacies C and D (Fig. 6) have a large extent. The latter exhibits a thickness of 250–300 m (Fig. 6, zone III). This hydrofacies outcrops at the Cerro de la Estrella, in the southern portion of zone I (Fig. 6).

In the upper portion of zone II (Fig. 6), hydrofacies A is interbedded with the other three hydrofacies, which may interrupt its continuity, while hydrofacies B and C are present at all depths, but as lenses interbedded with the other two

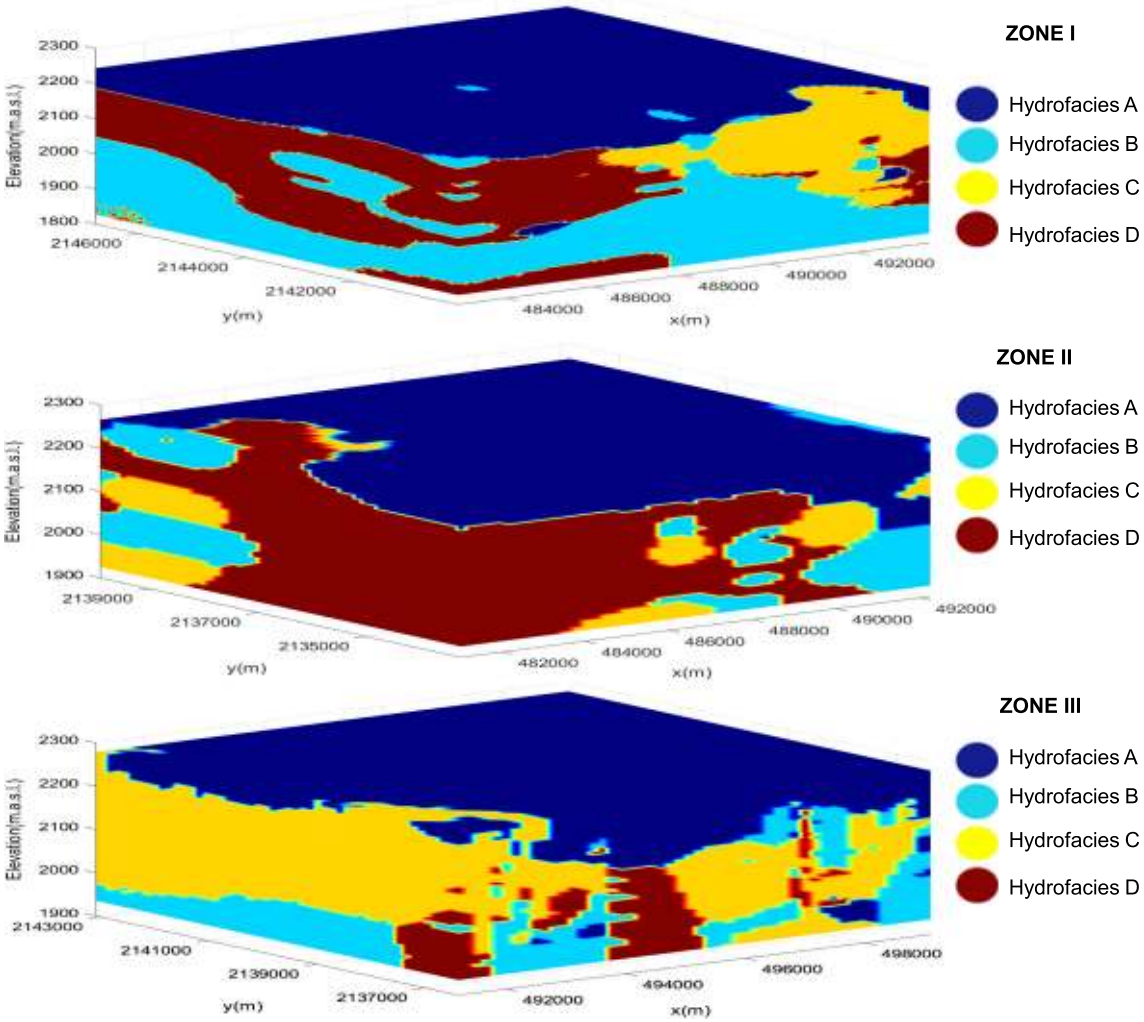

Fig. 6 Distribution of hydrofacies obtained by sequential indicator simulation (average of 1,000 realizations)

hydrofacies. Finally, hydrofacies D shows more continuity at the western portion of zone II, which corresponds to the lower parts of the Sierra de las Cruces (Fig. 1).

In zone III (Fig. 6), hydrofacies C presents some continuity at the south and west faces of the block. The west face corresponds to Cerro de la Estrella volcano, while the south face corresponds to Sierra Santa Catarina. Hydrofacies C is overlain by hydrofacies A, while hydrofacies B and D are interbedded in lower portion of the block.

Figure 7 compares the proportions obtained from data and those modeled for each hydrofacies in zone I. There is good agreement between observed and modeled proportions; similar results were obtained in the other two zones. An additional measure of the predictive capabilities of the models is obtained from computing the mismatch error between zones that overlap (Fig. 1). Since the computational grids were different for each zone, uniform grids of the overlapping volume, between zones I and II and between zones II and III, were constructed. The hydrofacies predicted in each zone was defined on the uniform grid (using the nearest neighbor) and a mismatch error was computed (one if the predicted hydrofacies were different, zero otherwise). The resulting mismatch between zones I and II is 31.65% and between zones II and III is 12.04%.

Figure 8 depicts the probability of occurrence of each hydrofacies in zone I for the corresponding model in Fig. 7. The effect of conditioning is evident in this figure, as two boreholes can be delineated near the SW limit of the domain, whose lithological records consist mainly of hydrofacies B and D. For these two hydrofacies, probability of occurrence is close to 1, while high probability of occurrence for hydrofacies A is limited to the upper portion of the wells and hydrofacies C was not present. It is also evident from this figure that at intermediate distance between these two wells the probability of occurrence of hydrofacies B and D is close to 0.5, defining a zone of large uncertainty in delineating the boundary between these two hydrofacies.

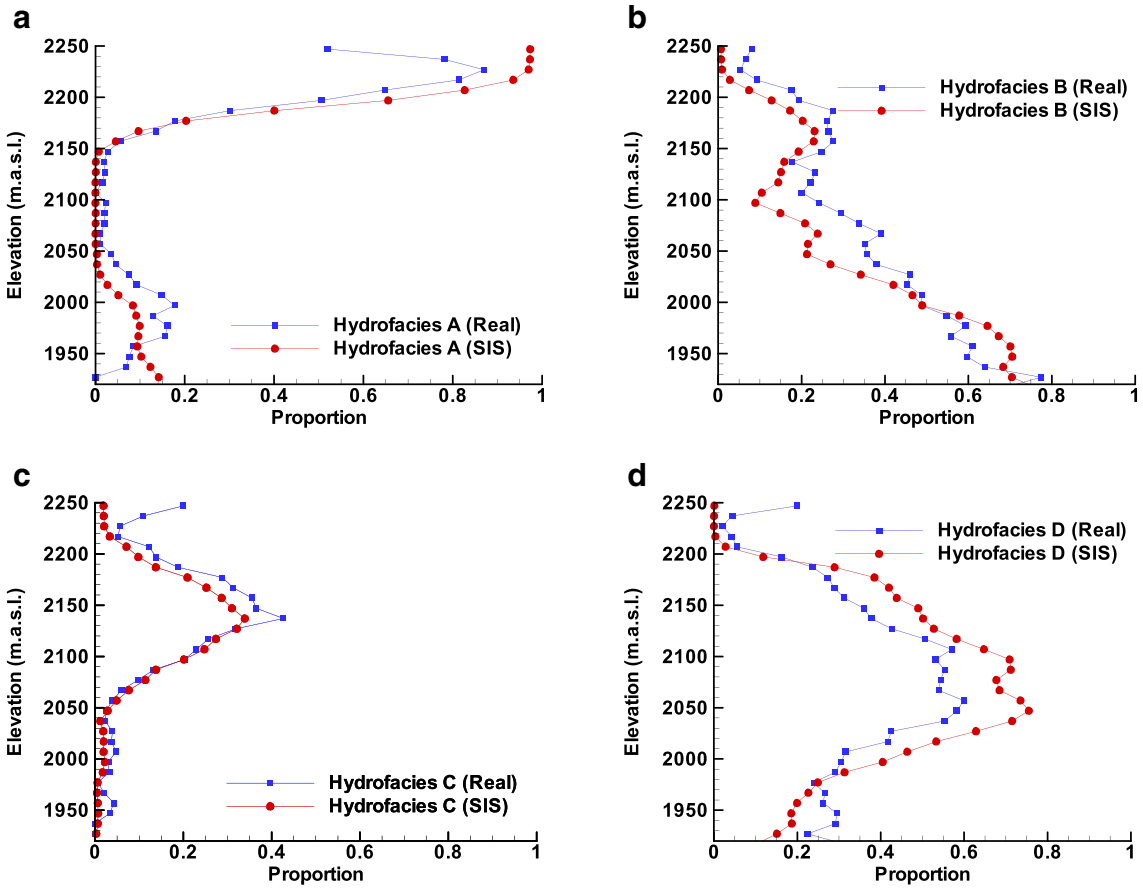

Fig. 7 Vertical proportions for hydrofacies in zone I from data (Real) and sequential indicator simulation (SIS). **a**–**d** Hydrofacies A, B, C and D

Discussion

A conceptual model is proposed based on the 3D distribution of hydrofacies. In this model, the main aquifer of Mexico City is composed of a complex set of hydrofacies with high- and low- hydraulic conductivities. To the authors' knowledge, this is the first application of sequential indicator simulation to model the distribution of hydrofacies in a volcano-sedimentary environment such as the hydrogeologic system in Mexico City. From a theoretical point of view, there is no difference in applying the method to the alluvial/glacio-fluvial and volcano-sedimentary cases. The differences are in the geological context. The vertical distribution of the sediments in glacial-fluvial environments is complex because their formation is the result of the interaction of previous and recent sediments with the movement of the glacier; hence, the sediments do not present the typical alternating sequence of alluvial environments. In the case of Mexico City, its geological evolution is the product of diverse volcanic episodes of varied composition that add an element of complexity to the sediments deposited in alluvial and lacustrine environments; thus, an alternating sequence between alluvial and volcanic materials would be restricted to the areas where volcanism was present or close to the source.

Figure 9 compares two geologic sections based on Vázquez-Sánchez and Jaimes-Palomera (1989), marked AA′ and BB′ in Fig. 1, and the distribution of hydrofacies obtained from the 3D models. The distribution of hydrofacies obtained from the borehole lithological data is more complex than what the geologic sections suggest. Adding complexity to this representation, each hydrofacies is heterogeneous in terms of hydrogeological parameters, particularly hydraulic conductivity, K. Vargas and Ortega (2004) conducted 225 tests in piezometers constructed in the lacustrine sediments in Mexico City; these lacustrine sediments correspond to hydrofacies A. K values in this data set range from 1×10^{-7} to 1×10^{-11} m/s with an arithmetic mean of 1.08×10^{-9} m/s. Medina-Ortega (2016) reinterpreted three pumping tests (only drawdown data at the pumping well was available for these tests) within the study area and estimated effective values of K for hydrofacies B, C and D at a nominal scale of 100 m (approximately the average length of the screen). Additional estimates of K for alluvial deposits (mostly hydrofacies D) and volcanic rocks (mainly hydrofacies C) from reinterpretation of pumping tests were reported by Instituto de Geofísica-UNAM (1994). Combining the results of these references, values of K for hydrofacies C range from 2.9×10^{-2} to 1×10^{-5} m/s. On the other hand, values of K for hydrofacies D range from $1 \times$

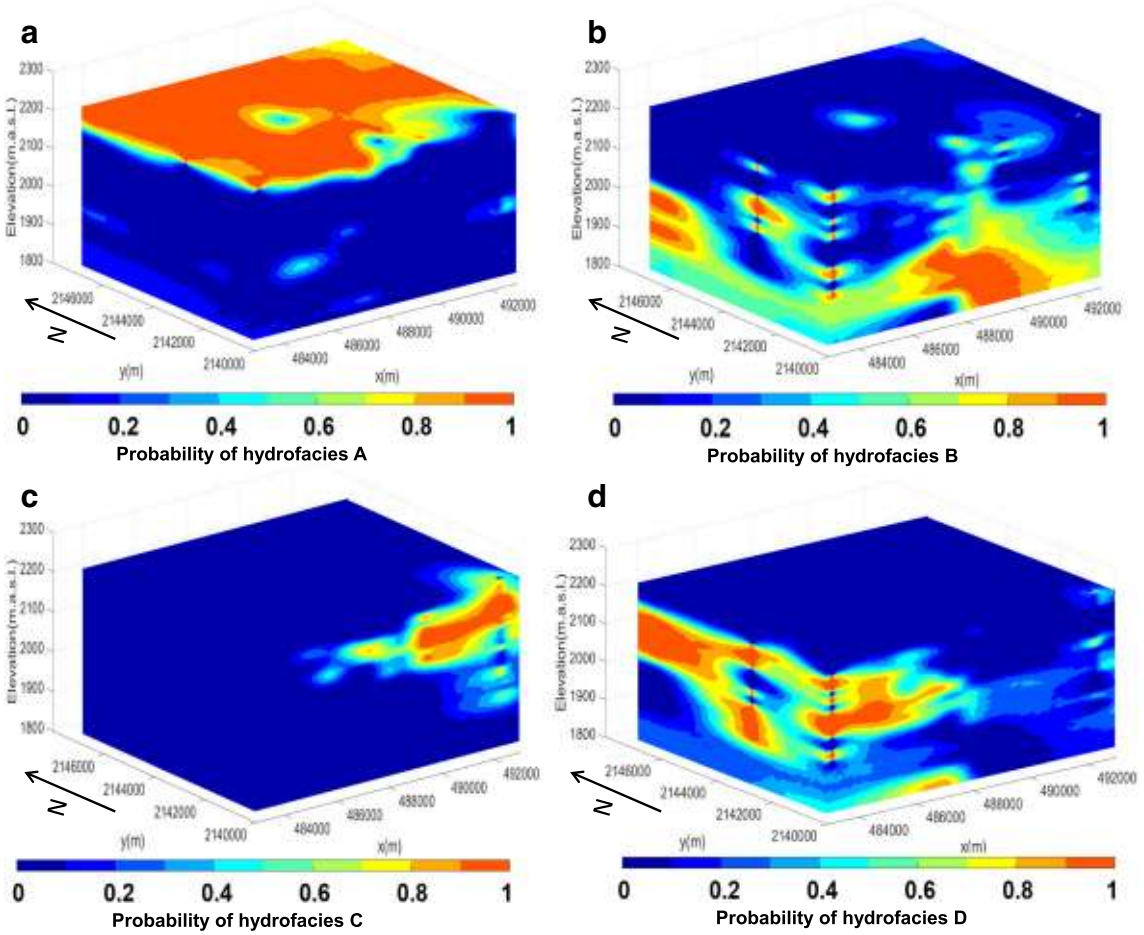

Fig. 8 Probability of occurrence of each hydrofacies in zone I. **a**–**d** Hydrofacies A, B, C and D

10^{-2} to 1×10^{-5} m/s. For hydrofacies B, Medina-Ortega (2016) estimates range from 1×10^{-3} to 4×10^{-9} m/s. Based on these estimates, a conceptual distribution of hydraulic conductivity (expressed as $Y = \ln K$) for each hydrofacies is shown in lower part of Fig. 9, highlighting their heterogeneous nature.

Wells supplying water to Mexico City are vulnerable due to sustained drawdown of piezometric levels, presence of contaminant sources in the urban area and land settlement (Escolero et al. 2016). There has been evidence of low water quality in the aquifer for several years (National Research Council 1995). Total and fecal coliforms, as well as bacteria responsible for gastroenteric diseases and acute diarrheas, have been found in groundwater in the southern and western parts of the city (Tortajada 2006). According to this author, the gastroenteric diseases, resulting from the consumption of polluted water, are the fourth major reason for child mortality in Mexico City (157/100,000). Nitrates are also a contaminant of concern in the southern portion of the city (Montiel-Palma et al. 2014). In addition, groundwater quality from wells in the municipality of Iztapalapa is degrading due to mixing with brackish groundwater from the aquitard (Domínguez-Marianai et al. 2015). This situation highlights the need of a wellhead protection program for wells supplying drinking water for Mexico City. The hydrofacies model developed in this study is a first step in describing the heterogeneity of the hydrogeologic system, and provides a physical framework to include in groundwater flow models for the delineation of wellhead protection areas. However, since the nominal scale of the present hydrofacies model is 1.45 km, additional on-site characterization of the heterogeneity (through exploratory drilling and geophysical investigation) would be needed. On the other hand, the scale of resolution of the hydrofacies model is adequate for regional and intermediate-scale groundwater modeling, to design water management strategies to attenuate drawdown of piezometric levels and subsidence rates.

Conceptually, it is well known that the volcanic materials are interbedded with the lacustrine and alluvial sediments (Vázquez-Sánchez and Jaimes-Palomera 1989; García-Palomo et al. 2008; Arce et al. 2015). However, no site-specific model for the aquifer of Mexico City existed up to now. The hydrofacies models (Fig. 6) provide site-specific 3D estimates of such complexity plus probability of occurrence of each hydrofacies (Fig. 8). These site specific

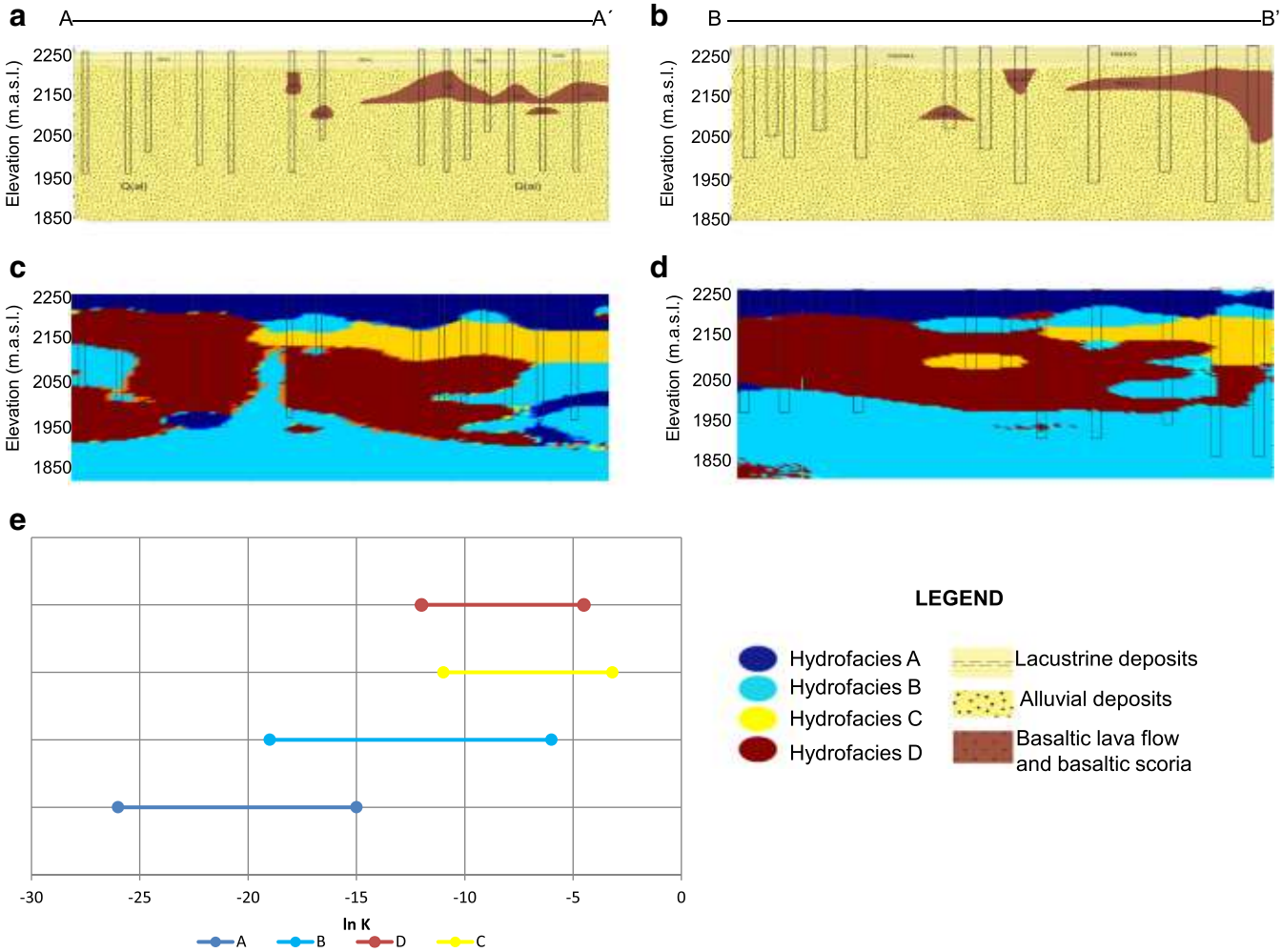

Fig. 9 Comparison between geological sections shown in Fig. 1: **a** section AA′ and **b** section BB′, and the corresponding simulated distribution of hydrofacies, **c** section AA′ and **d** section BB′. **e** Plot of the estimated range of ln *K* for each hydrofacies

hydrostratigraphic models provide a more detailed physical framework for understanding and modeling appearance of fractures and differential settlements. The hydrofacies model of zone II (Figs. 6 and 8) is roughly centered in the municipality of Iztapalapa, encompassing almost 50% of its territory. Extensive fracturing due to land subsidence and differential settlements has been mapped in this municipality (Carreón-Freyre et al. 2010), with an average length of 82 m per fracture (Carreón-Freyre et al. 2011). Approximately 60% of these fractures have an orientation NE–SW (Carreón-Freyre et al. 2011), roughly parallel to the contour of the Sierra Santa Catarina volcanic unit (Fig. 1). Future work should relate the distribution of volcanic hydrofacies with the appearance and development of fractures, and investigate the relation of the hydrostratigraphy and the spatial gradients in subsidence in Mexico City (Cabral-Cano et al. 2008).

Finally, another area that could benefit from a 3D hydrofacies model, is the modeling of the seismic response of a given site to an earthquake. The dominant period, which defines the seismic response of a given site, depends on the stratigraphy, the physical properties of the different geologic materials and the thickness of the lacustrine sediments (Ovando-Shelley et al. 2013; Arroyo et al. 2013). Efforts have been conducted to model and predict how the dominant periods of different areas in Mexico City change as the thickness of lacustrine sediments is diminished due to land subsidence (Avilés and Pérez-Rocha 2010; Arroyo et al. 2013). Although the hydrofacies model developed here is focused on hydraulic properties, it provides useful information about the stratigraphy of a specific site, and could be employed to improve the predictive capabilities of seismic-response models.

Conclusions

A 3D model for the distribution of four hydrofacies was obtained from a geostatistical indicator analysis of lithological records from groundwater wells. The spatial variability of the hydrofacies is the result of the geological evolution of the Basin of Mexico, where periods of volcanic activity alternate

with alluvial fans and lacustrine environments. As a result, Mexico City's hydrogeologic system is a complex, heterogeneous combination of alluvial material, volcanic rocks and lacustrine sediments. This complexity is simplified by grouping eleven lithological facies found in lithological records from groundwater wells into four hydrofacies. Hydrofacies A corresponds to lacustrine sediments of low hydraulic conductivity K; this hydrofacies overlies and semiconfines the main aquifer. In turn, the main aquifer (thickness of about 230 m) is composed of hydrofacies B (low K volcanic and volcano-sedimentary material), hydrofacies C (high K volcanic rocks) and hydrofacies D (high K alluvial sediments). Hydrofacies D is present in the entire aquifer in proportion from 30 to 50%, and it is interbedded with hydrofacies B and C. Hydrofacies C predominates in the upper 100 m of the aquifer (about 25% in average, but peaking at 50%), while hydrofacies B is more abundant in the lower 100 m of the aquifer (30–50%).

Site-specific quantitative analyses of hydrofacies would provide a well-informed prior estimate for statistics on the proportion, geometry, and juxtapositioning of facies in the facies assemblages expected to occur at the site. This information would fit in a hydrogeological decision analysis framework at a specific site such as the one outlined by Freeze et al. (1990). By incorporating the information obtained by a quantitative analysis of hydrofacies, the hydrogeological decision analysis would begin with a reduced level of uncertainty.

Acknowledgements The authors thank José Luis Lezama-Campos for elaborating the computational scripts for the geostatistical simulation and for processing and visualizing the data. Comments and suggestions by Martín Díaz-Viera, Peter Johnson and two anonymous reviewers were helpful for improving the manuscript.

Funding information This research was funded by grant IA101412-2 from UNAM-DGAPA-PAPIIT and by a scholarship from CONACYT to the leading author.

References

Arce JL, Layer PW, Morales-Casique E, Benowitz JA, Rangel E, Escolero OA (2013) New constraints on the subsurface geology of the Mexico City Basin: the San Lorenzo Tezonco deep well, on the basis of 40Ar/39Ar geochronology and whole-rock chemistry. J Volcanol Geothermal Res 266:34–49. https://doi.org/10.1016/j.jvolgeores.2013.09.004.

Arce JL, Layer PW, Martínez I, Salinas JI, Macías-Romo MC, Morales-Casique E, Benowitz JA, Escolero O, Lenhardt N (2015) Geología y estratigrafía del pozo profundo San Lorenzo Tezonco y de sus alrededores, sur de la Cuenca de México [Geology and stratigraphy of the San Lorenzo Tezonco deep well and its surroundings, south of the Basin of Mexico]. Bol Soc Geol Mexicana 67(2):123–143.

Arce JL, Layer PW, Macías JL, Morales-Casique E, García-Palomo A, Jiménez-Domínguez FJ, Benowitz J, Vásquez-Serrano A (2019) Geology and stratigraphy of the Mexico Basin (Mexico City), central Trans-Mexican Volcanic Belt. J Maps 15(2):320–332. https://doi.org/10.1080/17445647.2019.1593251

Arroyo D, Ordaz M, Ovando-Shelley O, Guasch JC, Lermo J, Perez C, Alcantara L, Ramírez-Centeno MS (2013) Evaluation of the change in dominant periods in the lake-bed zone of Mexico City produced by ground subsidence through the use of site amplification factors. Soil Dynam Earthquake Eng 44:54–66. https://doi.org/10.1016/j.soildyn.2012.08.009

Auvinet G (2009) Land subsidence in Mexico City. In: Auvinet GY, Juárez M (eds) Geotechnical engineering in urban areas affected by land subsidence. Volume prepared by ISSMGE Technical Committee 36 for XVII ISSMGE Conference, Alexandria, Egypt, vol 2009. Mexican Society of Soil Mechanics, Mexico City, pp 3–11

Avilés J, Pérez-Rocha LE (2010) Regional subsidence of Mexico City and its effects on seismic response. Soil Dynam Earthquake Eng 30(10):981–989. https://doi.org/10.1016/j.soildyn.2010.04.009

Cabral-Cano E, Dixon TH, Miralles-Wilhelm F, Díaz-Molina O, Sánchez-Zamora O, Carande RE (2008) Space geodetic imaging of rapid ground subsidence in Mexico City. GSA Bull 120(11–12):1556–1566. https://doi.org/10.1130/B26001.1

Carle SF, Fogg GE (1996) Transition probability-based indicator geostatistics. Mathematic Geol 28(4):453–476

Carle SF, Fogg GE (1997) Modeling spatial variability with one and multidimensional continuous-lag Markov chain. Mathemat Geol 29(7):891–918

Carreón-Freyre D, Cerca M, Gutiérrez-Calderón R, Huerta-Ladrón De Guevara M (2010) Monitoring of land subsidence and fracturing in Iztapalapa, Mexico City, In: Carreón-Freyre D, Cerca M, Galloway DL (eds) Land subsidence: associated hazards and the role of natural resources development. IAHS Publ. 339, IAHS, Wallingford, UK, pp 44–50

Carreón-Freyre D, González-Hernández M, Cerca M, Gutiérrez-Calderón R, Jiménez Sánchez CA (2011) Caracterización geomecánica de los suelos de Iztapalapa, México, para evaluar el fracturamiento causado por deformación diferencial [Geomechanical characterization of soils in Iztapalapa, México, to evaluate fracturing caused by differential deformation]. In: Conference Proceedings 2011 Pan-Am CGS Geotechnical Conference, Canadian Geotechnical Society, Richmond, BC, pp 1599–1606

Carrera-Hernández JJ, Gaskin SJ (2008) Spatio-temporal analysis of potential aquifer recharge: application to the Basin of Mexico. J Hydrol 353:228–246. https://doi.org/10.1016/j.jhydrol.2008.02.012

dell'Arciprete D, Bersezio R, Felletti F, Giudici M, Comunian A, Renard P (2012) Comparison of three geostatistical methods for hydrofacies simulation: a test on alluvial sediments. Hydrogeol J 20(2):299–311. https://doi.org/10.1007/s10040-011-0808-0

Deutsch CV, Journel AG (1998) GSLIB geostatistical software library and user's guide, 2nd edn. Oxford University Press, New York

Doherty J (2010) PEST, Model-independent parameter estimation: user manual, 5th edn. Watermark, Brisbane, Australia

Domínguez-Mariani E, Vargas-Cabrera C, Martínez-Mijangos F, Gómez-Reyes E, Monroy-Hermosillo O (2015) Determinación de los procesos hidrogeoquímicos participantes en la composición del agua de las fuentes de abastecimiento a pobladores de la delegación Iztapalapa, D.F., México [Determination of hydrogeochemical processes associated with the composition of water from supply wells for the inhabitants of the Iztapalapa District, D.F., Mexico]. Bol Soc Geol Mexicana 67(2):299–313. https://doi.org/10.18268/BSGM2015v67n2a12

Escolero O, Kralisch S, Martínez SE, Perevochtchikova M (2016) Diagnóstico y análisis de los factores que influyen en la vulnerabilidad de las fuentes de abastecimiento de agua potable a la Ciudad de México, México [Diagnosis and analysis of factors that affect the vulnerability of potable water supply sources to Mexico City, Mexico]. Bol Soc Geol Mexicana 68(3):409–427

Ezzedine S, Rubin Y, Chen J (1999) Bayesian method for hydrogeological site characterization using borehole and geophysical survey data: theory and application to the Lawrence Livermore National Laboratory Superfund Site. Water Resour Res 35(9):2671–2683

Fogg GE, Noyes CD, Carle SF (1998) Geologically based model of heterogeneous hydraulic conductivity in an alluvial setting. Hydrogeol J 6(1):131–143

Freeze RA, Massmann J, Smith L, Sperling T, James B (1990) Hydrogeological decision-analysis 1: a framework. Ground Water 28(5):738–766. https://doi.org/10.1111/j.1745-6584.1990.tb01989.x

García-Palomo A, Zamorano JJ, López-Miguel C, Galván-García A, Carlos-Valerio V, Ortega R, Macías JL (2008) El arreglo morfoestructural de la Sierra de Las Cruces, México central [The morphostructural arrangement of the Sierra de Las Cruces, central Mexico]. Rev Mexicana Cien Geol 25(1):158–178

He X, Koch J, Sonnenborg TO, Jørgensen F, Schamper C, Refsgaard JC (2014) Transition probability-based stochastic geological modeling using airborne geophysical data and borehole data. Water Resour Res 50. https://doi.org/10.1002/2013WR014593

Hernández-Espriú A, Reyna-Gutiérrez JA, Sánchez-León E, Cabral-Cano E, Carrera-Hernández J, Martínez-Santos P, Macías-Medrano S, Falorni G, Colombo D (2014) The DRASTIC-Sg model: an extension to the DRASTIC approach for mapping groundwater vulnerability in aquifers subject to differential land subsidence, with application to Mexico City. Hydrogeol J 22(6):1469–1485. https://doi.org/10.1007/s10040-014-1130-4

Instituto de Geofísica-UNAM (1994) Diagnóstico del estado presente de las aguas subterráneas de la Ciudad de México y determinación de sus condiciones futuras [Diagnosis of the current state of groundwater in Mexico City and determination of its future conditions]. Technical report for Departamento del Distrito Federal, Dirección General de Construcción y Operación Hidráulica, Mexico City, 110 pp

Jaime-P A, Méndez-Sánchez E (2010) Evolution of Mexico City clay properties affected by land subsidence. In: Carreón-Freyre D, Cerca M, Galloway DL, Silva-Corona JJ (eds) Land subsidence, associated hazards and the role of natural resources development. IAHS Publ. 339, IAHS, Wallingford, UK, pp 232–234

Johnson NM (1995) Characterization of alluvial hydrostratigraphy with indicator semivariograms. Water Resour Res 31(12):3217–3227

Johnson NM, Dreis SJ (1989) Hydrostratigraphic interpretation using indicator geostatistics. Water Resour Res 25(12):2501–2510

Jørgensen F, Høyera AS, Sandersen PBE, He X, Foged N (2015) Combining 3D geological modelling techniques to address variations in geology, data type and density: an example from southern Denmark. Comput Geosci 81:53–63. https://doi.org/10.1016/j.cageo.2015.04.010

Journel AG (1983) Nonparametric estimation of spatial distributions. Math Geol 15(3):445–468

Lozano-García S, Brown ET, Ortega B, Caballero M, Werne J, Fawcett PJ, Schwalb A, Valero-Garcés BL, Schnurrenberger D, O'Grady R, Stockhecke M, Steinman B, Cabral-Cano E, Caballero C, Sosa-Nájera S, Soler AM, Pérez L, Noren A, Myrbo A, Bücker M, Wattrus N, Arciniega A, Wonik T, Watt S, Kumar D, Acosta C, Martínez I, Cossio R, Ferland T, Vergara-Huerta F (2017) Perforación profunda en el lago de Chalco: reporte técnico [Deep drilling at the Chalco lake: a technical report]. Bol Soc Geol Mexicana 69(2):299–311. https://doi.org/10.18268/BSGM2017v69n2a2

Marsal RJ, Mazari M (1959) The subsoil of Mexico City, vol 377. Universidad Nacional Autónoma de México, Mexico City

Medina-Ortega P (2016) Modelo geoestadístico de hidrofacies y parametrización hidrogeológica de una porción del acuífero aluvial de la Ciudad de México [Geostatistical model of hydrofacies and hydrogeologic parameterization of a portion of the alluvial aquifer of Mexico City]. MSc Thesis, Universidad Nacional Autónoma de México, Mexico, 227 pp

Montiel-Palma S, Armienta-Hernández MA, Rodríguez-Castillo R, Domínguez-Mariani E (2014) Identificación de zonas de contaminación por nitratos en el agua subterránea de la zona sur de la Cuenca de México [Identification of zones contaminated by nitrate in groundwater in the southern portion of the Basin of Mexico]. Rev Internacional de Contaminación Ambiental 30(2):149–165

Morales-Casique E, Escolero OA, Arce JL (2015) Estimación de parámetros mediante inversión y análisis de las pérdidas hidráulicas lineales y no-lineales durante el desarrollo y aforo del pozo San Lorenzo Tezonco [Estimation of parameters using inversion and analysis of linear and non-linear hydraulic losses during the development and step-drawdown testing of the San Lorenzo Tezonco well]. Bol Soc Geol Mexicana 67(2):203–214. https://doi.org/10.18268/BSGM2015v67n2a5

Mooser F (2018) Geología del Valle de México y otras regiones del país, vol I [Geology of the Valley of Mexico and other regions of the country, vol 1], 1st edn. Colegio de Ingenieros Civiles de México, Mexico City

Moysey S, Caers J, Knight R, Allen-King RM (2003) Stochastic estimation of facies using ground penetrating radar data. Stochast Environ Res Asses 17(5):306–318. https://doi.org/10.1007/s00477-003-0152-6

National Research Council (1995) Mexico City's water supply: improving the outlook for sustainability. The National Academies Press, Washington, DC. https://doi.org/10.17226/4937

Ortega-Guerrero A, Rudolph DL, Cherry JA (1999) Analysis of long-term land subsidence near Mexico City: field investigations and predictive modeling. Water Resour Res 35(11):3327–3341

Ortega-Guerrero B, Lozano-García S, Herrera-Hernandez D, Caballero M, Beramendi-Orosco L, Bernal JP, Torres-Rodríguez E, Avendano-Villeda D (2017) Lithostratigraphy and physical properties of lacustrine sediments of the last ca. 150 kyr from Chalco basin, central Mexico. J South Am Earth Sci 79:507–524. https://doi.org/10.1016/j.jsames.2017.09.003

Ovando-Shelley E, Ossa A, Santoyo E (2013) Effects of regional subsidence and earthquakes on architectural monuments in Mexico City. Bol Soc Geol Mexicana 65(1):157–167

Poeter E, Gaylord DR (1990) Influence of aquifer heterogeneity on contaminant transport at the Hanford Site. Ground Water 28(6):900–909. https://doi.org/10.1111/j.1745-6584.1990.tb01726.x

Ritzi RW, Jayne DF, Zahradnik AJ, Field AA, Fogg GE (1994) Geostatistical modeling of heterogeneity in glaciofluvial, buried-valley aquifers. Ground Water 32(4):666–674. https://doi.org/10.1111/j.1745-6584.1994.tb00903.x

Ritzi RW (2000) Behavior of indicator variograms and transition probabilities in relation to the variance in lengths of hydrofacies. Water Resour Res 36(11):3375–3381

Ritzi RW, Dominic DF, Slesers AJ, Greer CB, Reboulet EC, Telford JA, Masters RW, Klohe CA, Bogle JL, Means BP (2000) Comparing statistical models of physical heterogeneity in buried-valley aquifers. Water Resour Res 36(11):3179–3192

Tortajada C (2006) Water management in Mexico City metropolitan area. Water Resour Develop 22(2):353–376. https://doi.org/10.1080/07900620600671367

Valencia-Cruz, NI (2002) Geología y correlación litoestratigráfica del subsuelo de la porción sur sureste del Valle de México. Facultad de Ingeniería, Universidad Nacional Autónoma de México, Mexico City, 85 pp

Vargas C, Ortega-Guerrero A (2004) Fracture hydraulic conductivity in the Mexico City clayey aquitard: field piezometer rising-head tests. Hydrogeol J 12(3):336–344. https://doi.org/10.1007/s10040-003-0302-4

Vazquéz-Sanchéz E, Jaimes-Palomera R (1989) Geología de la Cuenca de México [Geology of the Basin of Mexico]. Geofís Int 28(2):133–190

Zapata-Norberto B, Morales-Casique E, Herrera GS (2018) Nonlinear consolidation in randomly heterogeneous highly compressible aquitards. Hydrogeol J 26(3):755–769. https://doi.org/10.1007/s10040-017-1698-6